Automated interpretation of the coronary angioscopy with deep convolutional neural networks

Toru Miyoshi[1, 4], MD; Akinori Higaki[2, 3], MD, PhD; Hideo Kawakami[1], MD, PhD; Osamu Yamaguchi[2] MD, PhD

1) Department of Cardiology, Ehime Prefectural Imabari Hospital, Imabari, Japan.
2) Department of Cardiology, Pulmonology, Hypertension and Nephrology, Ehime University Graduate School of Medicine, Toon, Japan.
3) Hypertension and Vascular Research Unit, Lady Davis Institute for Medical Research, Sir Mortimer B. Davis Jewish General Hospital, McGill University, Montreal, Canada
4) Department of Cardiovascular Medicine, Osaka University Graduate School of Medicine, Suita, Japan.

Short title: Deep learning for coronary angioscopy

Word count: 2436 (excluding title page, abstract, references, figures and tables), **Figures:** 5, **Tables:** 0, **References:** 27

Keywords: Coronary angioscopy; Deep convolutional neural network; Generative adversarial networks; Artificial intelligence

Corresponding author:

Akinori Higaki MD, PhD

Hypertension and Vascular Research Unit,

Lady Davis Institute for Medical Research,

Sir Mortimer B. Davis-Jewish General Hospital,

McGill University,

Office F-139,

3755 ch. de la Côte-Sainte-Catherine, Montréal, Québec, H3T 1E2

Phone.: 514-340-8222, extension 22010

Email: akinori.higaki@mail.mcgill.ca

Abstract

Objective: Coronary angioscopy (CAS) is a useful modality to assess the atherosclerotic changes, but the interpretation of the obtained images requires expert knowledge. In this study, we showed the potential usage of deep convolutional neural networks (DCNN) for the diagnostic prediction and image synthesis.

Methods: 107 images from 47 patients, who underwent coronary angioscopy in our hospital between February 2014 and October 2017, and 864 images, selected from 142 MEDLINE-indexed articles published between April 2000 and April 2019, were used for the modeling. First, we developed a prediction model for the angioscopic findings. Next, we made a standard generative adversarial networks (GAN) model to simulate the CAS images. Finally, we tried control the output images according to the angioscopic findings with conditional GAN architecture.

Results: For both yellow color (YC) grade and neointimal coverage (NC) grade, we could observe strong and significant correlations between the true grades and the predicted values (YC grade, average r value = 0.80 ± 0.02, p-value <0.001; NC grade, average r value = 0.73 ± 0.02, $p < 0.001$). The binary classification model for the red thrombus yielded 0.71 ± 0.03 F_1-score. The average Inception score was 3.57 ± 0.06 in the images obtained from the standard GAN model. In the conditional GAN model, there were significant positive correlations between given values and the expert's diagnosis in YC grade and NC grade.

Conclusion: DCNN is useful in diagnostic prediction as well as in generating images from the findings in CAS.

Word count: 246 (abstract)

Introduction

Coronary angioscopy (CAS) is a unique imaging device which enables direct visualization of the vessel lumen and provides comprehensive information about the atherosclerotic changes (1, 2). It has been reported that CAS has a higher ability to detect neointimal vulnerability after the stent implantation than do other modalities (3). However, in spite of these advantages, this procedure is not commonly used in the daily clinical practice.

Currently, there is an increasing number of studies about the application of artificial intelligence in the field of cardiology (4). In particular, deep convolutional neural networks (DCNNs) have become popular in the medical image analysis (5, 6). DCNNs are also used for the generative modeling, such as generative adversarial network (GAN) (7). GAN algorithm learns the latent representation of the input data and outputs new datasets which have a similar distribution of the original data. With this ability, GAN is now used to complement missing data and transform image domains in the medical field (8). Therefore, we considered that this technology could be useful for the interpretation of the CAS findings. In this study, we developed a data-driven prediction model for the angioscopic findings as a first step. Next, we made a standard GAN model to synthesize realistic CAS images. Finally, we tried to control the output image of the generative model using conditional GAN architecture.

Methods

This retrospective observatory study was performed following the principles of the Declaration of Helsinki and the Japanese ethical guidelines for clinical research. All patients provided written informed consent. The study protocol was approved by the institutional review boards and the ethics committees of Ehime Prefectural Imabari Hospital. A part of the

datasets to replicate our study findings including public domain pictures and script files will be available from the online repository (http://dx.doi.org/10.17632/9dx23j5d64.1).

Image acquisition from patients

As a real-world data, we retrospectively assessed 107 consecutive lesions after stent implantation using CAS for 47 patients who had undergone PCI between February 2014 and October 2017 at Ehime Prefectural Imabari Hospital. Catheterization was performed with a radial, brachial or femoral approach using ≥6-F guiding catheters. CAS was performed with the FT-203F (FiberTech Co. Ltd., Tokyo, Japan) non-obstructive coronary angioscope system and the VISIBLE (FiberTech Co. Ltd.) optical fiber as previously reported (9).

Evaluation of the angioscopy

Each CAS analysis was performed as agreed by 2 independent cardiologists as shown in Fig 1. Neointimal coverage (NC) grade was evaluated using a 4-point grading scale, from 0 (no coverage) to 3 (complete coverage). Plaque yellow color (YC) was assessed using a 4-grade system, from 0 (white) to 3 (bright yellow). The presence of red thrombus was also assessed as previously described (10).

Additional image collection from MEDLINE-indexed articles

In order to address the small sample size, we also collected angioscopic images using PubMed search. We selected 142 MEDLINE-indexed articles which include coronary angioscopy pictures, published between April 2000 and April 2019. Pictures with excessive modifications or annotations (e.g. lines and arrows) were excluded from the analysis. All collected images were curated by at least two expert cardiologists. Since not all pictures were

obtained from the stent implanted site (especially in the older literatures), the NC grades were uniformly defined as 3 when stent struts were not observed.

Image data preprocessing

All collected images were converted to the Joint Photographic Experts Group (JPEG) format with 24-bit color data and resized to 96x96 pixels with the image processing tool of Python interpreter (Pillow; Alex Clark and Contributors). In order to increase the model's robustness, we applied data augmentation to the input data, in reference to the previous report (11). We invented four variants per each original picture; 45-, 135-, 225- and 315-degree rotation. For the appropriate cross-validation, the augmented data was separated into training and test datasets, so as not to share the same image source.

Structure of the prediction models

We designed a simple DCNN model which can be universally used for the assessment of yellow color grade, neointimal coverage grade and red thrombus. We used four convolution layers including batch normalization and put a fully connected layer in the final section. For the regression tasks (predicting the grade scores), we employed mean squared error as a loss function. For the binary classification, we set sigmoid function as the final activation function and used binary cross entropy as a loss function. Adaptive moment estimation (Adam) was used in the all prediction models as an optimization algorithm.

Structure of the GAN models

We designed the standard GAN model with convolution layers, in reference to the original article (12). Based on this model, we made some modification to construct the conditional GAN model as shown in Fig 1. All CAS findings were used as the conditioning information

to train the model. For the standardization, YC and NC grades were divided by three to be ranged between 0 and 1. The conditioning vector was concatenated with a gaussian noise and passed to the generator network. For the discriminator network, conditions were combined with the image data as input and also passed to the fully connected layer. Detailed descriptions and the source codes are available at the online repository

Evaluation method for the performance of GAN models

For the standard GAN model, Inception scores were calculated for randomly selected 1000 images from the original data and for the 1000 generated images respectively. We employed a blinded visual scoring system for the evaluation of the conditional GAN model. Two experts were asked to grade the generated pictures without any information about the given conditions. Per each grade, 8 images were generated by the conditional GAN. These blinded scores were compared with the given conditions and the correlation coefficient was calculated.

Statistical analysis

Data are presented as mean ± standard error. 5-fold cross validation was used to evaluate prediction models. For the assessment of regression models, we employed Pearson's correlation coefficient (r-value) and mean absolute error (MAE) as an indicator of the model performance. R-values higher than 7.0 were considered to show strong positive linear relationships. For the binary classification task, we used precision, recall and F_1-score as indicators. P-values less than 0.05 were regarded as statistically significant. All analysis was performed using SciPy module in the python library.

Results

Patient characteristics enrolled in our hospital

In the total 47 patients from which we obtained CAS images, 32 (68%) was male. The mean age of the cohort was 70.2 ± 1.3 years old and 24 (51%), 34 (72%) and 24 (51%) cases have diabetes mellitus, hypertension and dyslipidemia respectively. Seven patients (15%) were smokers. Average HbA1c level was 6.4 ± 0.1 %. All patients were prescribed acetylsalicylic acid and 43 (91%) were receiving dual antiplatelet therapy. 8 patients (17%) was receiving anticoagulant therapy with warfarin. 43 patients were taking statins and the average low-density lipoprotein cholesterol level was 89.2 ± 4.2 mg/dL. Serum creatinine level was 1.2 ± 0.2 mg/dL in average. Among 44 patients who were treated with drug eluting stents, 1 case was with paclitaxel-eluting stent, 9 cases were with sirolimus-eluting stents, 14 cases were with everolimus-eluting stents and 18 cases were with zotarolimus-eluting stents. Only 2 patients (4%) were implanted bare metal stents. Mean stent length was 22.5 ± 1.6 mm and the mean diameter was 3.4 ± 0.4 mm. The mean follow-up period from the first treatment was 14.6 ± 2.9 months. 51% of the observed lesions was left anterior descending artery and 36% was the right coronary artery.

Characteristics of the articles in the PubMed search

Total 864 different angioscopic images were obtained from 142 articles. Among these 142 articles, 82 (57.7%) were the original articles and 44 (30.9%) were the case reports. 12 review articles, 2 letters, a rapid communication and an editorial article were also included. Among them, 89 (62.7%) articles provide the images of stented lesions, and the rest are about the de novo lesions. On average, 7.1 pictures were available from one original article and 4.4 pictures from a case report. *Circulation Journal* (29 articles, 20.4%), *JACC Cardiovascular Intervention* (16 articles, 11.3%) and *International Journal of Cardiology* (9 articles, 6.3%) were the top 3 most frequently found journals through the online search.

Distributions of CAS findings

In our hospital data, the most frequently observed finding was YC grade 0, NC grade 1 without any thrombus (17.8% of the total 107 images). YC grade 3 was not observed except in NC grade 3 without thrombus. Red thrombi were most frequently observed in YC grade 1, NC grade 1 area (Fig 2A). On the other hand, YC grade 0, NC grade 1 is the most frequent finding among the images collected through PubMed search (16.2% of the total 864 images). (Fig 2B). On the whole, lower NC grades were more frequently found in the published articles' pictures. Distribution in the mixed data is shown in Fig 2C.

Diagnostic prediction model for the angioscopic findings with DCNN

In both YC grade and NC grade prediction model, we could observe strong and significant correlations between the true grades and the predicted values (YC grade, average r value = 0.80 ± 0.02, p-value <0.001, average MAE = 0.16 ± 0.01; NC grade, average r value = 0.73 ± 0.02, $p < 0.001$, average MAE = 0.17 ± 0.01). Representative scatter plots were shown in Fig 3. The binary classification model for the red thrombus gave 0.87 ± 0.03 in precision and 0.60 ± 0.05 in recall, resulting in 0.71 ± 0.03 F_1-score.

3.5. Synthesized CAS images by the GAN models

For the standard GAN architecture, we could obtain a variety of angioscopic images (Fig 4A) with the average Inception score of 3.57 ± 0.06. This score was significantly lower than the one from the original dataset (3.90 ± 0.01, $p<0.01$). Using the conditional GAN architecture, we could control the output images by giving the conditions as shown in Fig 4B. There were significant and strong correlation between given conditions and experts' score in YC grades (r

value = 0.89, $p<0.001$). Significant correlation was also observed in NC grades, but the coefficient was lower than in YC grades (r value = 0.67, $p<0.001$).

Discussion

Coronary angioscopy (CAS) is a useful device which allows direct visualization of internal surface of the lumen, providing the information of characteristics of plaque and thrombus. Previously, we presented evidences that some CAS findings correspond to the pathological change (13) and give explanation for the other imaging modality such as optical coherence tomography (2). Angioscopy is also a useful follow up tool to for the stent implanted lesions (14). However, due to the limited medical resources, CAS remains an extraordinary procedure and mostly used for the research purposes. Along with the recent advancement in machine learning algorithms, there are increasing number of reports concerning the application of the artificial neural network to diagnostic imaging (15). In particular, deep generative modeling including GAN has emerged as an effective approach to simulate the complex data structure of the medical images (16-19). We recently reported that deep convolutional encoder-decoder model can be used to reconstruct the apical 2-chamber view in echocardiogram (20). Considering the DCNN's ability to expand the potential of diagnostic modalities, we thought that such technologies can be also applicable to broaden the usage of CAS. In this study, we demonstrated the potential use of DCNN for the interpretation of CAS views through both prediction task and generative modeling.

In this study, we first evaluated the performance of diagnostic prediction models. As previously discussed, one of the principal problems of the deep learning in the health science field is the paucity of large training dataset (21). In order to address this issue, we used MEDLINE database to collect angioscopic images and obtained 8 times bigger data. As

expected, the distribution patterns of the CAS findings were different between our hospital data and literature data; the latter showed broader distribution, which might increase the model's generalization capacity. Owing to this online database search, the trained models could achieve acceptable performance in YC grade and NC grade prediction. On the other hand, the sensitivity for the red thrombus detection model was not satisfactory. This might be ascribed to the relatively low incidence of the red thrombus (24% of the total images). Actually, there are rooms for further improvement in the model design, because we employed almost the same neural network architecture for the three different prediction tasks, for the sake of simplicity. In any case, this result is indicative that DCNN has a potential for the automated interpretation of CAS images. We next developed a generative model with GAN algorithm. Medical image simulation is one of the practical applications of the image synthesis with GAN. For example, Tom F et al. proposed a novel approach to simulate the intravascular ultrasound images with a stacked GAN based framework, with the belief that simulation model can serve as an aid for doctors to learn rare diseases (22). In line with this concept, we tried to obtain the realistic CAS images. It has been reported that simulation-based training improves the cardiology fellows' skills in the cardiac catheterization (23). Since the realistic visualization is an essential component of the practical simulation (24), our approach to generate CAS images with GAN should be a promising option for the medical simulation method. In this study, we also showed that conditional GAN is useful to control the output images according to the angioscopic findings. We could change the YC and NC grades of the output image at the same time, by giving the multi-dimensional condition. Although GANs with multiple input conditions were already reported (25), its application to the diagnostic imaging is still challenging. Therefore, we think our results can contribute to the future development of virtual coronary angioscopy (26).

There are several limitations in this study. First, we have to admit that this combined dataset is not reflective of the contemporary cohort of the coronary artery disease patients, because the therapeutics for the coronary intervention experienced a drastic change over the last couple of decades. Second, we only used Inception score as the quantitative evaluation for the performance of the GAN model. The most reasonable way to assess the reality of the synthesized images should be the visual Turing test (27), but it was not applicable in this study due to the relatively low image resolution. If we can collect much more data in the future, we can address this issue by employing more advanced algorithms.

Conclusion

DCNN are useful in diagnostic prediction as well as in generating images from the findings in CAS.

Acknowledgments

None

Sources of funding

None

Disclosures

Authors (TM, AH, HK and OY) have nothing to disclose concerning the submitted work.

Reference

1. Thieme T, Wernecke KD, Meyer R, Brandenstein E, Habedank D, Hinz A, et al. Angioscopic evaluation of atherosclerotic plaques: validation by histomorphologic analysis and association with stable and unstable coronary syndromes. Journal of the American College of Cardiology. 1996;28(1):1-6.

2. Miyoshi T, Kawakami H, Seike F, Oshita A, Matsuoka H. Relationship between yellow plaque grade and tissue protrusion after stent implantation: A coronary angioscopy study. J Cardiol. 2017;70(4):342-5.

3. MacNeill BD, Lowe HC, Takano M, Fuster V, Jang IK. Intravascular modalities for detection of vulnerable plaque: current status. Arterioscler Thromb Vasc Biol. 2003;23(8):1333-42.

4. Seetharam K, Shrestha S, Sengupta PP. Artificial Intelligence in Cardiovascular Medicine. Curr Treat Options Cardiovasc Med. 2019;21(6):25.

5. Betancur J, Hu LH, Commandeur F, Sharir T, Einstein AJ, Fish MB, et al. Deep Learning Analysis of Upright-Supine High-Efficiency SPECT Myocardial Perfusion Imaging for Prediction of Obstructive Coronary Artery Disease: A Multicenter Study. J Nucl Med. 2019;60(5):664-70.

6. Zhang J, Gajjala S, Agrawal P, Tison GH, Hallock LA, Beussink-Nelson L, et al. Fully Automated Echocardiogram Interpretation in Clinical Practice. Circulation. 2018;138(16):1623-35.

7. Goodfellow I, Pouget-Abadie J, Mirza M, Xu B, Warde-Farley D, Ozair S, et al., editors. Generative adversarial nets. Advances in neural information processing systems; 2014.

8. Cohen JP, Luck M, Honari S. Distribution Matching Losses Can Hallucinate Features in Medical Image Translation. arXiv preprint arXiv:180508841. 2018.

9. Dai K, Matsuoka H, Kawakami H, Sato T, Watanabe K, Nakama Y, et al. Comparison of Chronic Angioscopic Findings of Bare Metal Stents, 1st-Generation Drug-Eluting Stents and 2nd-Generation Drug-Eluting Stents- Multicenter Study of Intra-Coronary Angioscopy After Stent (MICASA). Circ J. 2016;80(9):1916-21.

10. Nishimoto Y, Ueda Y, Sugihara R, Murakami A, Ueno K, Takeda Y, et al. Comparison of angioscopic findings among second-generation drug-eluting stents. J Cardiol. 2017;70(3):297-302.

11. Perez L, Wang J. The effectiveness of data augmentation in image classification using deep learning. arXiv preprint arXiv:171204621. 2017.

12. Radford A, Metz L, Chintala S. Unsupervised representation learning with deep convolutional generative adversarial networks. arXiv preprint arXiv:151106434. 2015.

13. Miyoshi T, Kawakami H, Oshita A, Matsuoka H. A case of in-stent restenosis with pathologically proven chronic inflammation seven years after sirolimus-eluting stent implantation. J Cardiol Cases. 2017;15(5):176-9.

14. Miyoshi T, Matsuoka H, Kawakami H, Dai K, Sato T, Watanabe K, et al. Assessment of Second- and Third-Generation Drug-Eluting Stents on Chronic Coronary Angioscopy-Multicenter Study on Intra-Coronary AngioScopy After Stent (MICASA) Prospective Data Analysis. Circ J. 2018;82(7):1830-5.

15. Sengupta PP, Huang YM, Bansal M, Ashrafi A, Fisher M, Shameer K, et al. Cognitive Machine-Learning Algorithm for Cardiac Imaging: A Pilot Study for Differentiating Constrictive Pericarditis From Restrictive Cardiomyopathy. Circ Cardiovasc Imaging. 2016;9(6).

16. Ben-Cohen A, Klang E, Raskin SP, Amitai MM, Greenspan H, editors. Virtual PET images from CT data using deep convolutional networks: initial results. International Workshop on Simulation and Synthesis in Medical Imaging; 2017: Springer.

17. Galbusera F, Bassani T, Casaroli G, Gitto S, Zanchetta E, Costa F, et al. Generative models: an upcoming innovation in musculoskeletal radiology? A preliminary test in spine imaging. Eur Radiol Exp. 2018;2(1):29.

18. Nie D, Trullo R, Lian J, Petitjean C, Ruan S, Wang Q, et al., editors. Medical image synthesis with context-aware generative adversarial networks. International Conference on Medical Image Computing and Computer-Assisted Intervention; 2017: Springer.

19. Wolterink JM, Dinkla AM, Savenije MH, Seevinck PR, van den Berg CA, Išgum I, editors. Deep MR to CT synthesis using unpaired data. International Workshop on Simulation and Synthesis in Medical Imaging; 2017: Springer.

20. Higaki A, Inoue K, Kinoshita M, Ikeda S, Yamaguchi O. Reconstruction of Apical 2-Chamber View From Apical 4-and Long-Axis Views on Echocardiogram Using Machine Learning—Pilot Study With Deep Generative Modeling—. Circulation Reports. 2019:CR-19-0011.

21. Pasini A. Artificial neural networks for small dataset analysis. J Thorac Dis. 2015;7(5):953-60.

22. Tom F, Sheet D, editors. Simulating patho-realistic ultrasound images using deep generative networks with adversarial learning. 2018 IEEE 15th International Symposium on Biomedical Imaging (ISBI 2018); 2018: IEEE.

23. Schimmel DR, Sweis R, Cohen ER, Davidson C, Wayne DB. Targeting clinical outcomes: Endovascular simulation improves diagnostic coronary angiography skills. Catheter Cardiovasc Interv. 2016;87(3):383-8.

24. Wu J, Wang H, Zhang P, Ma X, Hu Q. A preliminary real-time and realistic simulation environment for percutaneous coronary intervention. Biomed Res Int. 2015;2015:183157.

25. Yildirim G, Seward C, Bergmann U. Disentangling Multiple Conditional Inputs in GANs. arXiv preprint arXiv:180607819. 2018.

26. Schroeder S, Kopp AF, Ohnesorge B, Loke-Gie H, Kuettner A, Baumbach A, et al. Virtual coronary angioscopy using multislice computed tomography. Heart. 2002;87(3):205-9.

27. Geman D, Geman S, Hallonquist N, Younes L. Visual Turing test for computer vision systems. Proc Natl Acad Sci U S A. 2015;112(12):3618-23.

Figure legends

Fig 1. Difinitions of coronary angioscopic images. Panel A shows the representative images for each yellow color (YC) grades. Panel B is for the neointimal coverage (NC) grades. All images shown are already converted to 96x96 pixels.

Fig 2. Schematic representation of the conditional GAN model. CAS findings are converted to condition vector and passed to both generator and discriminator networks.

Fig 3. Heatmaps for the distribution of the angioscopic findings. The percentage of the population with the specific finding was shown for the images obtained from our hospital (A), PubMed search (B) and in the merged dataset (C). In each area of the matrix, the right sided cell indicates the population with red thrombus. Cells with higher percentage were highlighted with red background color as a heatmap (colors are assigned independently for each panel).

Fig 4. Representative scatter plots from the 5-fold cross-validation. The correlation between observed values and predicted values in yellow grade score (A) and neointimal coverage score (B). A coefficient of determination is shown in each plot as R^2. Regression lines are also indicated.

Fig 5. Representative output images. Panel A shows representative output images of the standard GAN model. In panel B, longitudinal axis corresponds to the gradual change of neointima coverage grade and the horizontal axis indicates the grade of yellow color. The thrombus conditions were randomly assigned.

A

Yellow color grade (YC grade)

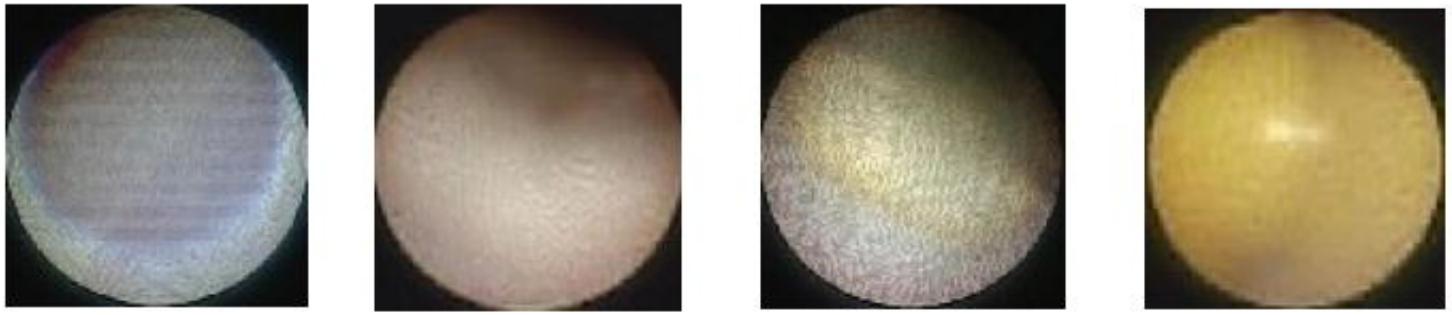

Grade 0 Grade 1 Grade 2 Grade 3

B

Neointimal coverage grade (NC grade)

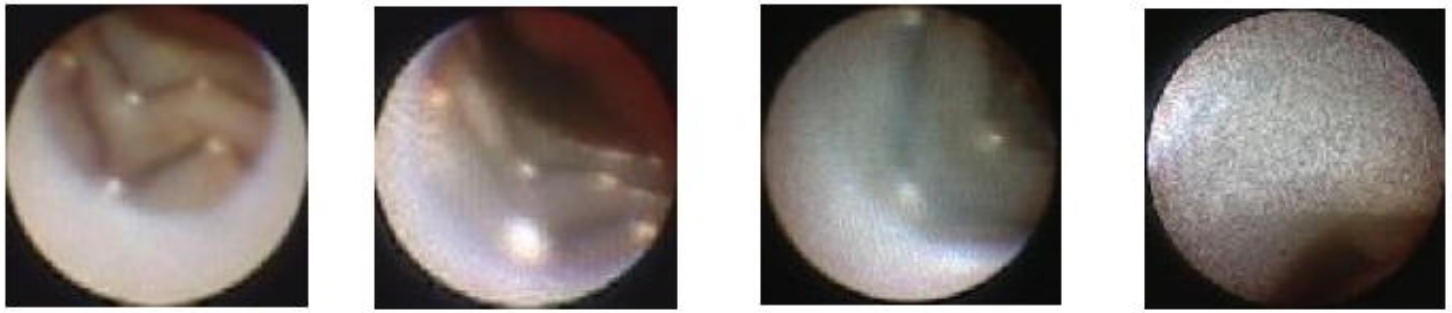

Grade 0 Grade 1 Grade 2 Grade 3

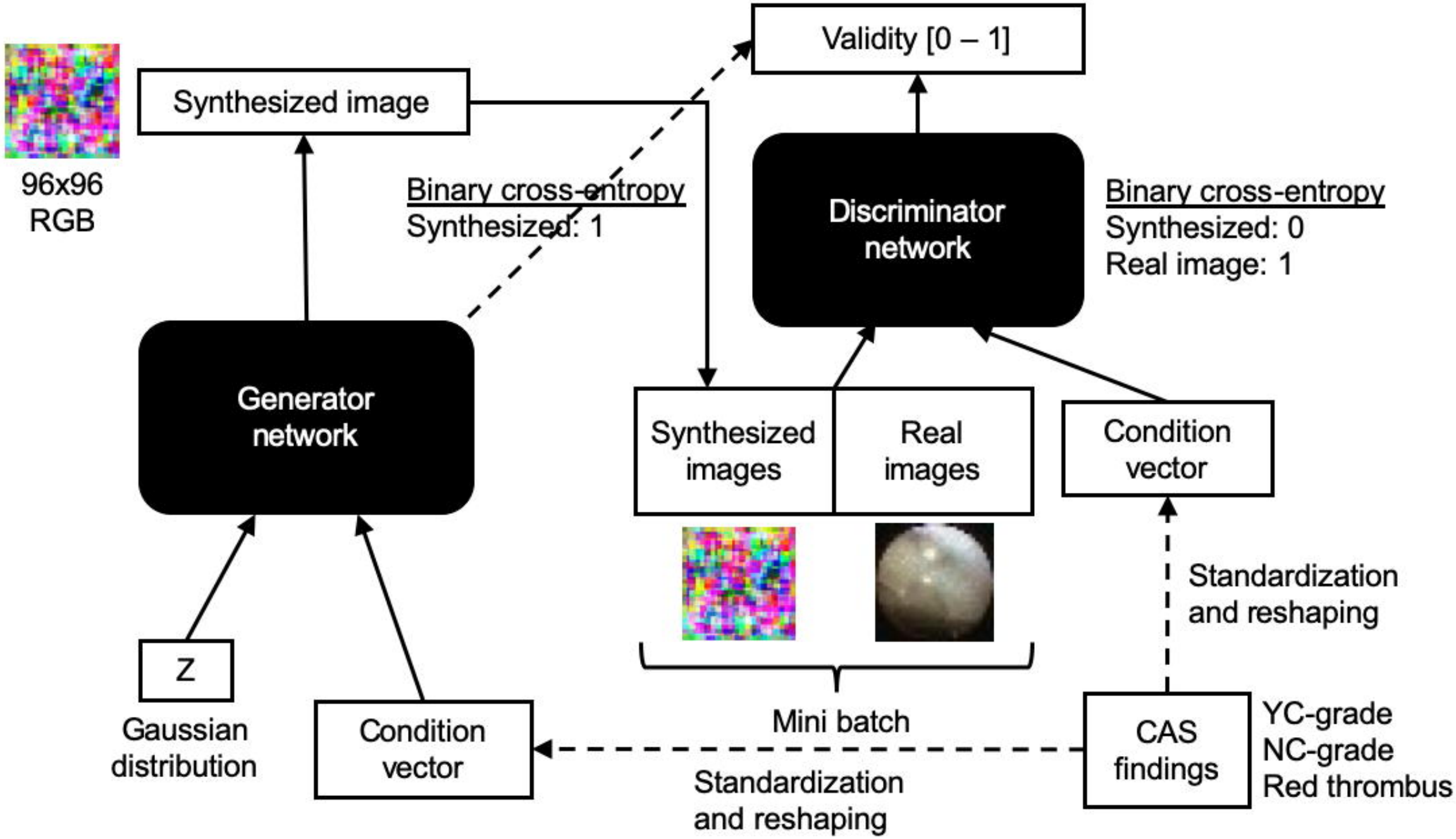
Validity [0 – 1]
Synthesized image
96x96
RGB
Binary cross-entropy
Synthesized: 1
Discriminator network
Binary cross-entropy
Synthesized: 0
Real image: 1
Generator network
Synthesized images
Real images
Condition vector
Standardization and reshaping
Z
Gaussian distribution
Condition vector
Mini batch
CAS findings
YC-grade
NC-grade
Red thrombus
Standardization and reshaping

A

Neointimal coverage	Yellow color grade / Red thrombus(-/+)							
	0		1		2		3	
3	4.7%	0.9%	9.3%	0.0%	8.4%	1.9%	3.7%	0.0%
2	9.3%	0.9%	8.4%	0.0%	7.5%	1.9%	0.0%	0.0%
1	17.8%	0.0%	3.7%	3.7%	13.1%	1.9%	0.0%	0.0%
0	0.0%	0.9%	1.9%	0.0%	0.0%	0.0%	0.0%	0.0%

B

Neointimal coverage	Yellow color grade / Red thrombus(-/+)							
	0		1		2		3	
3	16.2%	0.7%	9.6%	3.4%	10.0%	6.1%	7.6%	2.7%
2	6.3%	1.0%	5.8%	2.5%	4.6%	2.8%	1.2%	0.2%
1	2.2%	0.2%	3.0%	2.0%	2.7%	1.6%	0.2%	0.2%
0	1.6%	0.2%	1.9%	0.2%	1.5%	0.9%	0.5%	0.3%

C

Neointimal coverage	Yellow color grade / Red thrombus(-/+)							
	0		1		2		3	
3	16.8%	0.8%	10.8%	3.4%	11.0%	6.4%	8.1%	2.7%
2	7.4%	1.2%	6.8%	2.5%	5.6%	3.0%	1.2%	0.2%
1	4.4%	0.2%	3.5%	2.4%	4.3%	1.9%	0.2%	0.2%
0	1.6%	0.3%	2.1%	0.2%	1.5%	0.9%	0.5%	0.3%

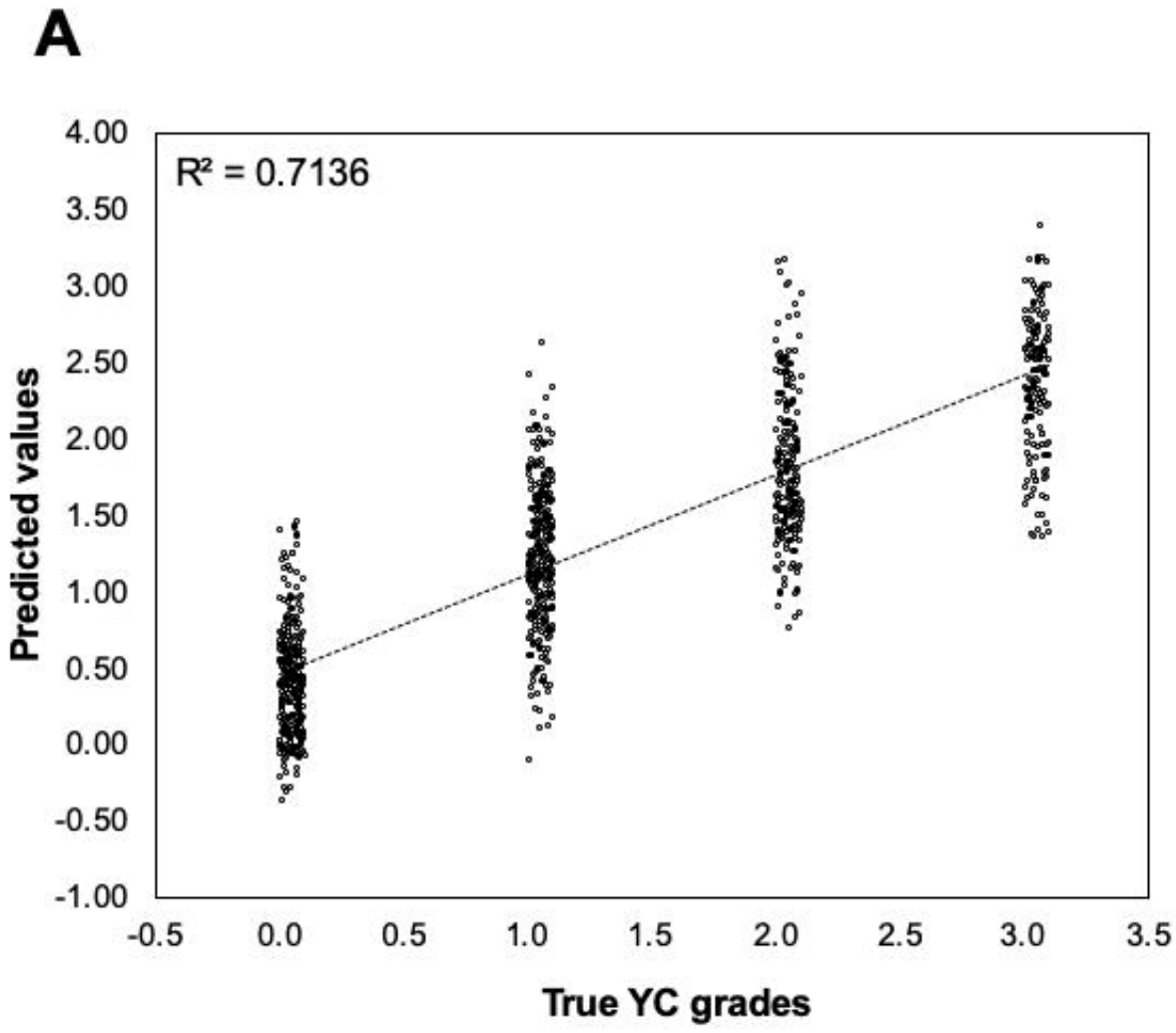
A
R² = 0.7136
Predicted values
True YC grades
4.00
3.50
3.00
2.50
2.00
1.50
1.00
0.50
0.00
-0.50
-1.00
-0.5
0.0
0.5
1.0
1.5
2.0
2.5
3.0
3.5

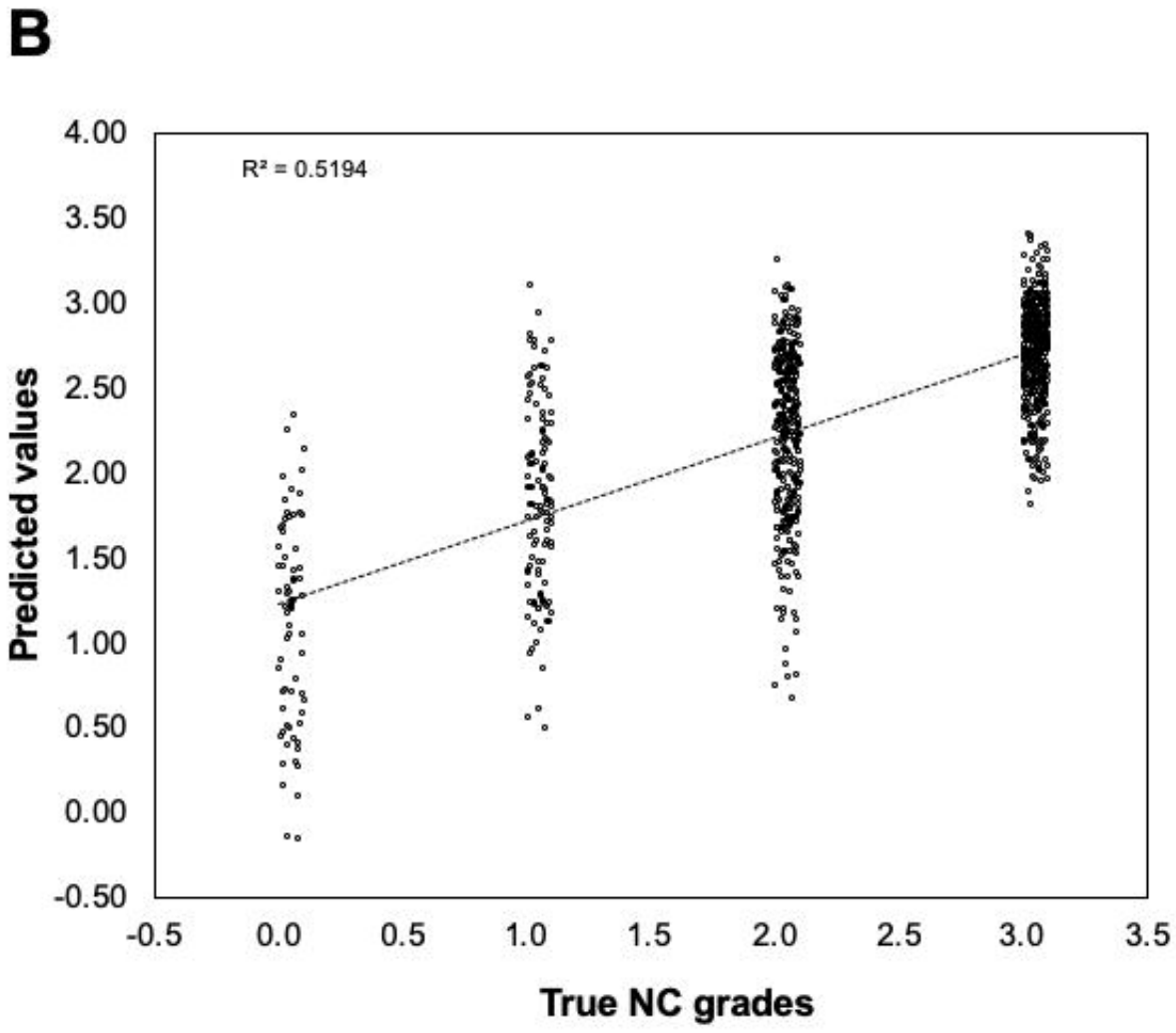
B
R² = 0.5194
Predicted values
True NC grades
4.00
3.50
3.00
2.50
2.00
1.50
1.00
0.50
0.00
-0.50
-0.5
0.0
0.5
1.0
1.5
2.0
2.5
3.0
3.5

A

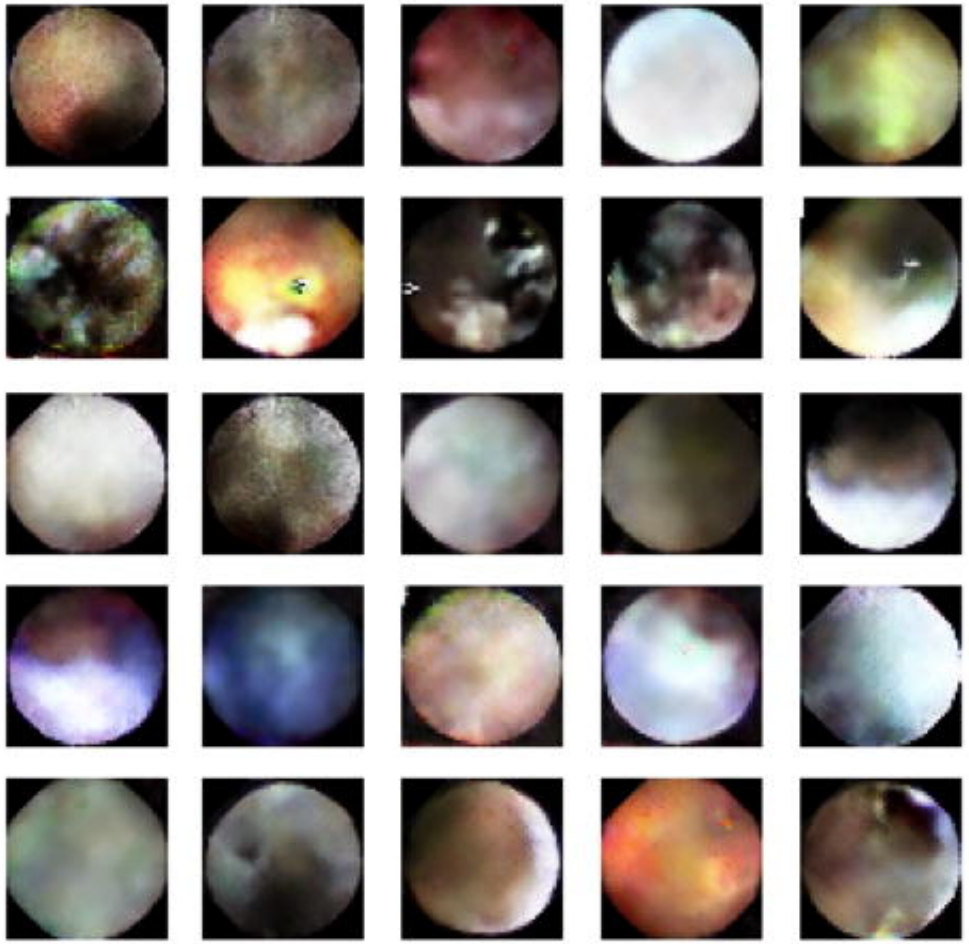
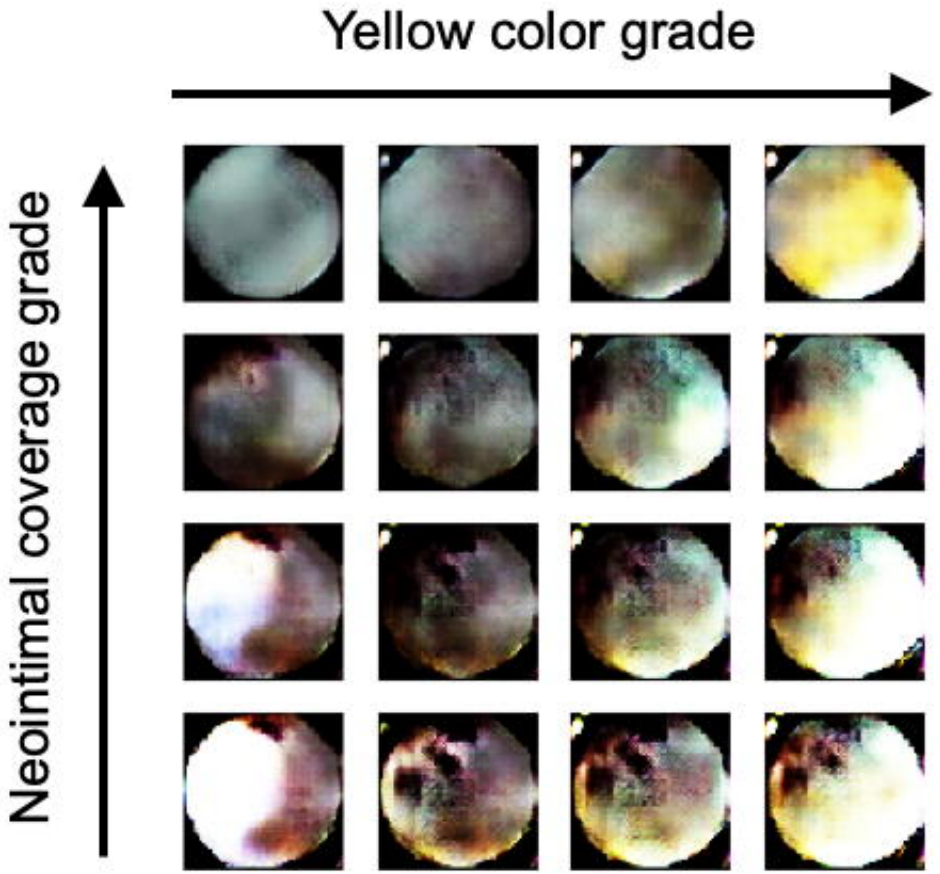
B